

# Investigations on the structure and properties of palm leaf sheath fiber

Tonghua Zhang · Min Guo · Lan Cheng · Xiaolong Li

Received: 13 June 2014 / Accepted: 2 February 2015 / Published online: 12 February 2015  
© Springer Science+Business Media Dordrecht 2015

**Abstract** As a natural cellulosic fiber, palm leaf sheath fiber (palm fiber) is widely-distributed and abundant cellulose and engineering fiber resource. To obtain essential information about palm fiber, its morphology, composition, chemical and crystal structure, tensile characteristic and adsorption property were investigated. Test results of palm fiber were compared with those of other natural cellulosic fibers. Palm fiber presents aligned Si-dots on the surface and abundant fiber cells with spiral vessel tissues at the cross section. The chemical composition reveals that palm fiber contains abundant lignin but smaller amount of cellulose (the content of 28.16 %). In addition, investigation illustrates that cellulose in palm fiber is  $I_{\beta}$ -dominant type, which is also confirmed by FTIR analysis. X-ray diffraction study shows that the crystallinity (30.52 %), crystallinity index (36.5 %) and crystal size (2.5 nm) are all apparently lower than those of ramie, flax and bamboo fibers. Given the low crystallinity and cellulose content of palm fiber, its tensile strength and Young's modulus are also lower than those of other fibers. Moreover, palm fiber exhibits

excellent breaking elongation, high moisture regain, distinct yield characteristic, and variability in strength. The modified Weibull model was used to study the tensile behavior of palm fiber. This model accurately predicted fiber strength. The absorption volume in isotherm of carbonized palm fiber increases with rising pressure, thus indicating good porous structure of the fiber.

**Keywords** Palm fiber · Structure · Crystallinity · Tensile property · Adsorption

## Introduction

Given increasing environmental concerns, scientists and technologists have placed considerable importance on the applications of natural fibers because of their substantial and sustainable advantages (Methacanon and Sumransin 2010; Summerscales et al. 2010). Palms (Arecaceae), widely distributed plants in the world, are commonly used for landscaping, decorations, and household items. Studies on palm have focused on the medical and technical use of palm oil, fruits, leaves, and seeds, as well as on its growth habit in agriculture, role in ecology, and genetic engineering (Zhang et al. 2010; Devshony et al. 1992; Maunder et al. 2001). The leaf sheath of palm and its fibers have been used to make raincoats as early as in the Han Dynasty (BC 202–220). In the Jin Dynasty (265–420), people spun palm fibers into ropes (Zhai 2010) because of the excellent hardness and antibacterial property of these fibers. Nowadays,

---

Tonghua Zhang and Min Guo are the first author of this study.

---

T. Zhang (✉) · M. Guo · L. Cheng  
College of Textiles and Garments, Southwest University,  
Chongqing 400715, People's Republic of China  
e-mail: zhtonghua@aliyun.com

X. Li  
Chongqing Three Gorges University, Chongqing 404120,  
People's Republic of China

manufacturers produce crafts and mattresses by using leaf sheath fibers of palm with several advantages, such as using natural raw materials, having desirable elasticity, and satisfying the requirements of human body mechanics (Dai 2008). It can be learnt that palm fiber exhibits good properties. Its intrinsic features, such as structural aspects, as well as tensile and chemical properties, are critical to fiber properties and applications. These properties have received increasing attention from investigations on natural fiber materials. However, unlike extensively studied jute, sisal, flax, ramie, and bamboo fibers (d’Almeida et al. 2006), studies on palm fiber are rare. Available knowledge, exploration, and utilization of palm fiber remain limited.

In general, palm fiber interweaves into networks, thus forming palm barks and covering palm trunks, layer upon layer. Fibers are manually pulled out from palm barks. In our previous work (Zhang et al. 2010), we revealed the simple but unique morphological structure of palm fiber, i.e., it has a rough, irregular, and uneven longitudinal surface that is similar to a cover of scale-like materials. In addition, the cross section of palm fiber is nearly circular and has numerous hollow sieve tubes. Considering that the natural hierarchical structure of palm fiber is different from other common fibers, further studies on palm fiber are valuable.

In the present study, the detailed morphological structure of palm fiber was elucidated. The crystallinity and chemical structure of palm fiber were characterized via X-ray diffraction (XRD) and Fourier transform infrared (FTIR) spectroscopy, respectively. The chemical composition, tensile and adsorption properties of palm fibers were investigated, and prominent features were discussed.

According to literature (Silva et al. 2008, 2010), natural fibers exhibit varying tensile strengths. The strength scatter of palm fiber was quantified by the Weibull distribution in this study. Palm fiber was also carbonized and analyzed by using a gas apparatus to obtain the adsorption isotherm and pore distribution of the hollow inner structure.

## Experimental

### Material

Palm barks were peeled directly from palm trees by using a knife. The barks were washed and rubbed manually

with water to remove dirt (Fig. 1a). Palm fibers were pulled from the palm barks after the barks were oven dried. Without pretreatment, the fibers exhibited different diameters, lengths, and hardness (Fig. 1b, c).

### Structural studies

The cross-sectional and surface morphological micrograms of palm fiber were obtained by using a scanning electron microscope (S-4800, Hitachi, Ltd., Japan). Meanwhile, a transmission electron microscope (TEM, H-7500, Hitachi, Ltd., Japan) was used to analyze the fiber cell structure of palm fiber.

### Chemical composition

The chemical composition of palm fiber was analyzed in accordance with the procedure of GB5889-86 *Ramie chemical composition quantitative analysis method*, which provides the percentages of cellulose, hemicellulose, and lignin in palm fiber.

### FTIR spectral analysis

FTIR was obtained by using a TENSOR 27 instrument (Bruker Corporation, USA) to analyze the functional groups and chemical structure of palm fiber.

### X-ray diffraction

X-ray trace was obtained by using a MSAL-XD3 XRD system (Micro Structure Analytical Laboratory, China) with  $\text{CuK}\alpha$  ( $\lambda = 1.5418 \text{ \AA}$ ) to describe the crystal structure and evaluate the crystallinity of palm fiber. Palm fiber powder which is 0.2 mm in diameter was tested. The X-ray generator system was operated at 40 kV and 30 mA. The  $2\theta$  angles ranged from  $7^\circ$  to  $50^\circ$ . The degree of crystallinity was calculated from diffraction intensity data by using deconvolution method. The diffraction data was fitted by Gaussian function through PeakFit program from  $7^\circ$  to  $40^\circ$  of  $2\theta$  degree to find the contribution of the crystalline cellulose peaks and the amorphous background. The degree of crystallinity  $X_c$  can be expressed as Eq. (1) (He et al. 2007; Focher et al. 2001):

$$X_c = \left( 1 - \frac{S_a}{S_a + S_{cr}} \right) \times 100 \quad (1)$$



**Fig. 1** **a** The palm-bark; **b** fibers with larger diameters, longer lengths and more hardness; **c** fibers with smaller diameters, shorter lengths and less hardness

where,  $S_a$  is the amorphous integrated area, and  $S_{cr}$  is the sum of the area of crystalline cellulose peaks.

### Tensile Property

The tensile test for palm fiber was performed according to ASTM D3379-75 (Guo et al. 2014; Munawar et al. 2007) with four different gauge lengths (GLs) 10, 20, 30, and 40 mm. The tests were conducted on a universal material tester (WDW3050) at 0.5 mm/min cross-girder rate, which corresponds to quasistatic tensile behavior (Belaadi et al. 2013) as strain rate increases from  $2.083 \times 10^{-4}$ /s (GL = 40 mm) to  $8.333 \times 10^{-4}$ /s (GL = 10 mm) in the linear region of the stress–strain curve. A total of 50 samples were tested at each GL. To calculate the cross area and strength of the tested palm fibers, their diameter was measured under a digital biological microscope (Axioskop 40, Carl Zeiss AG, Germany) within the GL area.

### Adsorption property

#### Moisture absorption

The moisture regain of palm fiber was investigated based on GB/T 9995-1977 *Determination of textile materials' moisture content and moisture regain* by drying the fibers (1 g) at 105 °C in a hot-air oven for 1 h. The fibers were then allowed to regain moisture under standard testing conditions of RH 65 % and 20 °C. The weight of the fibers was recorded every 5 min until the fibers achieved moisture sorption equilibrium. The moisture regain value was then calculated.

#### Moisture liberation

The fibers (1 g) were left in a glass desiccator with water at the bottom (RH 100 %) for 72 h to attain moisture sorption equilibrium. The subsequent calculation procedure was the same as that for moisture absorption.

## Results and discussion

### Structure of palm fiber

The morphology of palm fiber is shown in Fig. 2 at different magnifications. Palm fiber can be regarded as a subcylindrical shape and is covered by randomly distributed scale-like materials on the rough surface (Fig. 2a). These scale-like materials are organic, and d'Almeida et al. (2006) reported that the materials are possibly produced through fiber extraction from palm trees. At high magnification (Fig. 2b), palm fiber exhibits a clean area on the surface apart from the organic residue; protruded characteristics with arrays of protrusions/particles in particular holes are shown on the fiber surface. Such feature is also observed in several palm family fibers (Zhai 2010). From EDS analysis (d'Almeida et al. 2006), the protrusions are identified as thorn-ball-shaped Si-rich particles (called Si-dots). Christina et al. (2004) indicated that Si-dots are recorded outside vascular bundles or fine fibers in discontinuous or continuous distribution along the fiber axes, and Si-dots form compact structures with excellent antibacterial property.

Figure 3 shows vessels and phloem tissues (conducting tissues) accompanied by numerous elongated individual hollow palm fiber cells with diameters

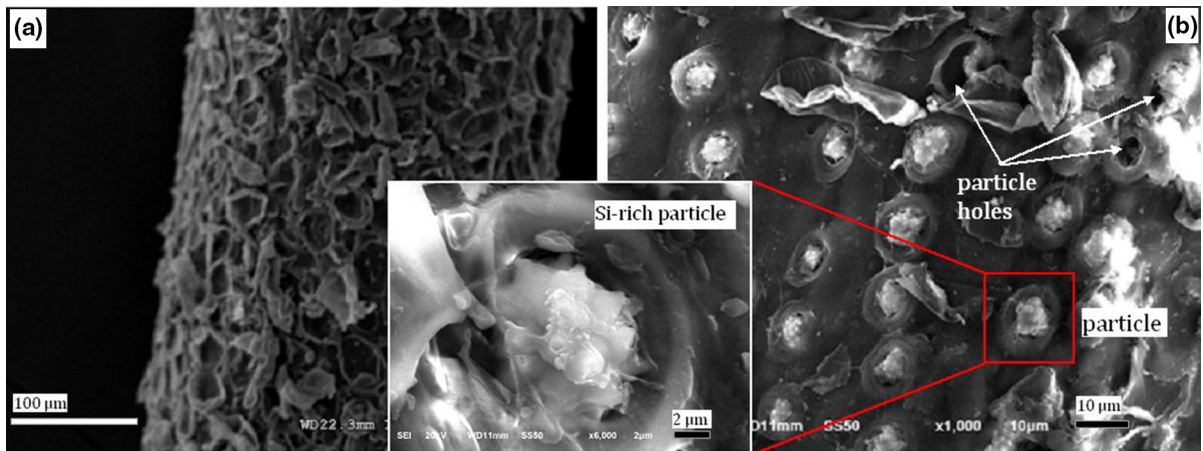


**Fig. 2** **a** The surface morphology of palm fiber; **b** the particles on the surface

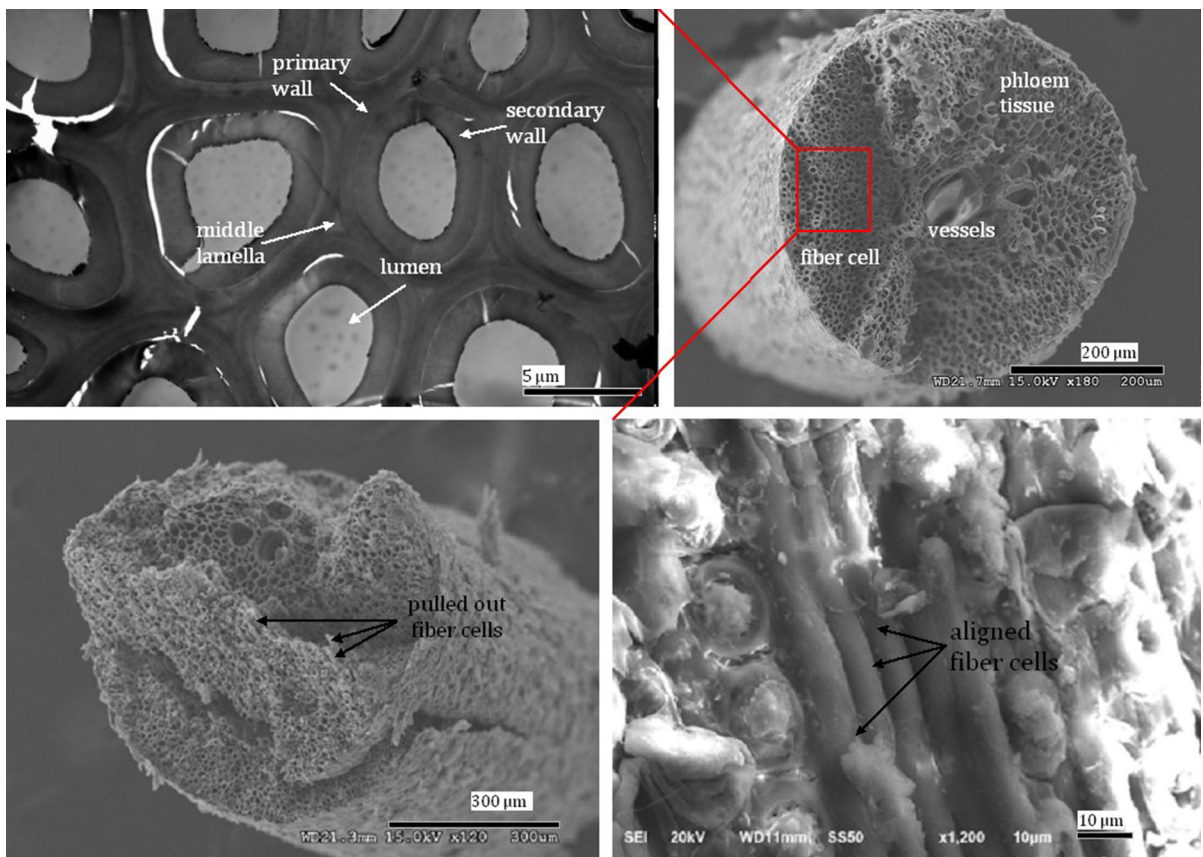


**Fig. 3** The cross-sectional structure and fiber cell of palm fiber

ranging from 6.10 to 11.57 μm (Guo et al. 2014) to exhibit honeycomb-like cross sections. Fiber cells are called sclerenchyma in botany, and they are tightly

connected with one another. The TEM micrograms in Fig. 3 show that fiber cells comprise the lumen, primary wall, and secondary wall. Studies reveal that

the secondary wall has three layers (Cheng et al. 2014), i.e., S1, S2, and S3 from the primary wall to the lumen; S2 determines the thickness of the cell wall. The middle lamella is the tissue that links fiber cells; this tissue consists of lignin and hemicellulose. Fiber cells grow parallel to the longitudinal direction because parallel pulled-out cells are found on the fracture surface and aligned fiber cells on the fiber surface. Such unidirectional, regular, and hollow structure provides palm fiber with potential applications in adsorption and filter engineering.

Figure 4 indicates that to a certain extent, vessels can be identified as fiber cells even though they are different in terms of size, shape, and wall thickness. Figure 4a shows the spiral characteristics within the vessels, and an individual exposed vessel with relatively even stripes is found in Fig. 4b. Figure 4c shows the SEM micrograph of a manually torn palm fiber sample. Parallel elongated fiber cells are found beside a broken vessel, which shows a spiral curve. Vessels in plant exhibit various patterns: spiral, scalariform, reticulate, pitted, and annular. Vessels in palm and sisal fibers are obviously spiral (Silva et al. 2009). Fiber strength decreases with increasing diameter because a large diameter indicates the existence of large vessels (Baley 2002). Given that vessels have a larger diameter but thin cell wall, fiber strength decreases.

Natural composite materials, such as grass, wood, and bone (Greenberg et al. 1989), have provided essential information on composite development because of their ideal structures. Palm fiber exhibits a hierarchical composite structure, which can be modeled as a three-component natural composite system that consists of reinforcements of fiber cells (sclerenchyma) and vessels, matrix of the middle lamella, and thin-walled fiber cells. This particular structure is believed to endow palm fiber with its unique properties.

#### Fiber composition

The main substances of palm fiber and some of the most commonly used cellulosic and palm family fibers are listed in Table 1.

Palm family fibers possess similar compositions. The obtained results revealed that palm fiber exhibits the lowest cellulose content. Differing from the single cell fiber such as cotton, palm and other fibers in

Table 1 can be considered as natural composites and need binding materials (especially lignin and hemicellulose) to hold several cells together. Palm fiber contains a high level of lignin, which is slightly lower than that of piassava. Except palm family fibers, even the highest one (jute) only contains 30.1 % of the amount of lignin of studied palm fiber. On account of abounding in lignin, palm fiber is yellow in color and uneven in fiber fineness (Wang et al. 2010). The hemicellulose content is rather high, approximately 20.60 % of the total mass of palm fiber.

#### FTIR analysis

Figure 5a shows the FTIR spectra of palm fiber determined at 620–4,000  $\text{cm}^{-1}$  wavenumber. The spectra is similar to that of other natural fibers with cellulose I structure, such as sisal (Cordeiro et al. 2011) and flax (Cantero et al. 2003).

The characteristic absorption peaks of cellulose at 2,924.5 and 2,853.2  $\text{cm}^{-1}$  correspond to the unsymmetrical stretching vibration of  $-\text{CH}_3$  and the symmetrical stretching vibration of  $-\text{CH}_2$ , respectively. An unsymmetrical stretching vibration exhibits a larger percentage than a symmetrical vibration in palm fiber. The strong absorption peak at 1,030.2  $\text{cm}^{-1}$  and the other two characteristic peaks of cellulose at 1,161.6 and 1,119.4  $\text{cm}^{-1}$  are all ascribed to the stretching vibration of three C–O bonds in a cellulosic glucose ring. The peak that is centered at 1,734.2  $\text{cm}^{-1}$ , character of hemicellulose, is attributed to the stretching vibration of C = O in acetyl groups. The absorbance at 1,614.8 and 1,520.3  $\text{cm}^{-1}$  caused by aromatic nucleus vibration, the peak at 1,669.2  $\text{cm}^{-1}$  associated with conjugate carbonyl, and the band at 1,456.5  $\text{cm}^{-1}$  assigned to the C–H bending vibration in methyl and methylene are all characteristic peaks of lignin (Li and Song 2005). The peak at 1,243.3  $\text{cm}^{-1}$  is attributed to lilac ring C–O stretching vibration, and no obvious absorption peak of the guaiac-based ring or hydroxybenzene is found near 1,243.3  $\text{cm}^{-1}$ . Thus, the main structure of lignin in palm fiber is based on syringyl units. The characteristic absorption peak of  $\beta$ -glycosidic linkage contributed by both cellulose and hemicellulose in the fiber is found at 895.5  $\text{cm}^{-1}$  (Mortazavi and Moghadam 2010).

The second derivative FTIR spectra of palm fiber in the OH group stretching and finger print region is

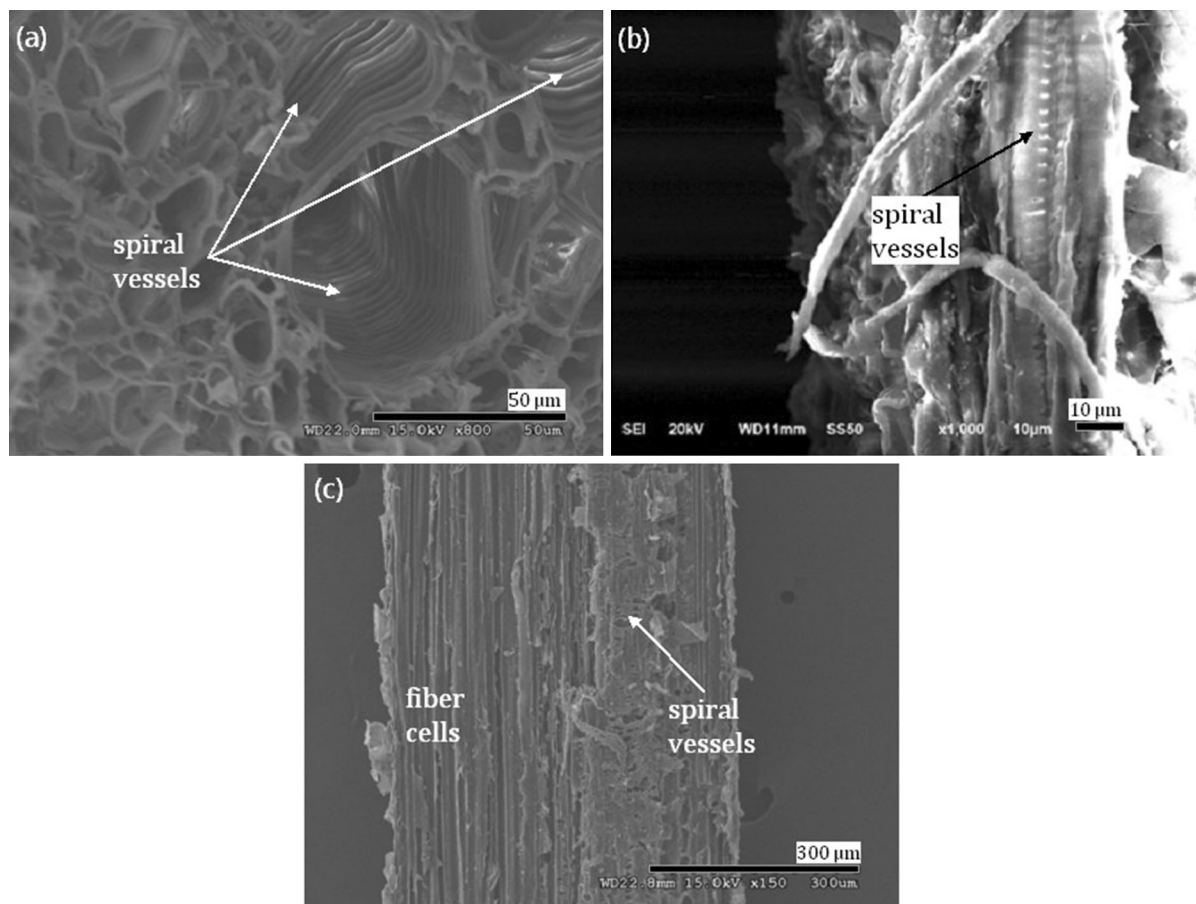


**Fig. 4** The spiral vessels of palm fiber

**Table 1** Crystallinity and chemical composition of palm fiber and other natural cellulosic fibers (Cordeiro et al. 2011; Wang et al. 2010; He et al. 2007)

Fibers	Cellulose (%)	Lignin (%)	Hemicellulose (%)	Crystallinity (%)		$L_{200}$ (nm)
				$X_c$	$I_c$	
Palm	28.16	44.07	20.60	30.52	36.5	2.5
Ramie	67–76	0.6–0.7	13–16	68.98	88.86	6.8
Bamboo	73.83	10.15	12.49	68.26	87.79	7.1
Flax	78.05	2.78	11.62	64.15	80.82	5.4
Coir	32–53	38–45	0.15–15			
Piassava	29	45	26			
Jute	68.39	13.3	13.53			
Sisal	60–75	8–12	10–15			

shown in Fig. 5b. It is known that cellulose I is composite of two distinct crystalline forms: cellulose  $I_\alpha$  (triclinic) and cellulose  $I_\beta$  (monoclinic) (O’Sullivan 1997), differing with the origin of cellulose samples in their relative amounts. Sugiyama et al. (1991) have

assigned the bands near 3,240 and 3,270  $\text{cm}^{-1}$  to cellulose  $I_\alpha$  and  $I_\beta$  phase respectively. Predominant cellulose  $I_\beta$  phase can be found from relative intensity of the two bands (He et al. 2007), corresponding to 3,235 and 3,274  $\text{cm}^{-1}$  in palm fiber. Such result can be

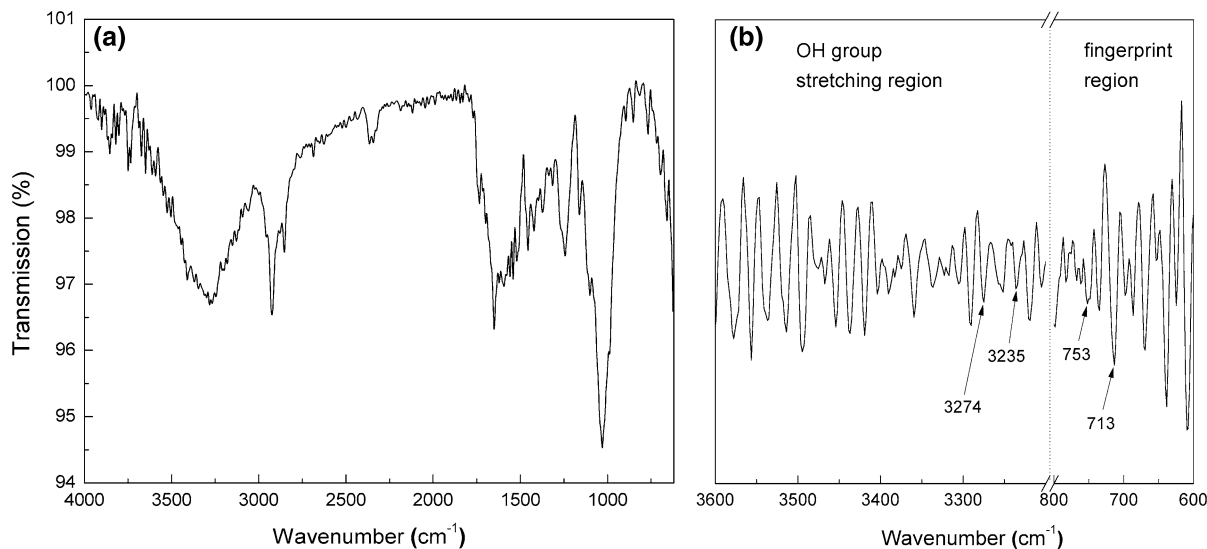


**Fig. 5** FTIR spectra (a) and second derivative FTIR spectra (b) of palm fiber

also verified in fingerprint region of second derivative FTIR spectra. Reports (He et al. 2007; Sugiyama et al. 1991) showed that bands near 750 and 710  $\text{cm}^{-1}$  was thought to be attributed to crystalline  $I_{\alpha}$  and  $I_{\beta}$  phase. It is suggested that palm fiber is cellulose  $I_{\beta}$ -dominant type from bands located at 753 and 713  $\text{cm}^{-1}$ .

Moreover, several characteristic absorption peaks of organic Si can be obtained from the FTIR spectra of palm fiber (Fig. 5a). In particular, the strong absorption peak at 1,030.2  $\text{cm}^{-1}$  corresponds to the stretching vibration of the Si–O–C bond. The peak located at 766  $\text{cm}^{-1}$  indicates the stretching vibration of Si–C. The medium-intensive broad bands observed around 895.5 and 848  $\text{cm}^{-1}$  are attributed to the association between Si and –OH and Si–O stretching vibration, respectively (Jiang and He 1992). The presence of Si-containing materials confirms the existence of Si-dots on palm fiber surface, which agrees with EDS results in the literature (d’Almeida et al. 2006).

#### Crystallinity and crystal structure analysis

The wide-angle XRD pattern of the palm fiber (Fig. 6) is very similar to that of coir and piassava fibers (Tomczak 2007; d’Almeida et al. 2006). In Fig. 6, the Miller indices are adopted. Simulation was carried out by using Mercury 3.3 and cellulose  $I_{\beta}$  powder structure (cellulose.cif file) was obtained from CCDC database (French 2014; Ganner et al. 2014). The characteristic

peaks of cellulose  $I_{\beta}$  have Miller indices of (1-10), (110), (200) and (004), corresponding to 15.36°, 16.42°, 22.43° and 34.52° of palm fiber. SEM and FTIR results told that palm fiber contains Si-dots, in addition,  $\text{SiO}_2$  was suggested to exist in those dots. XRD patterns of  $\text{SiO}_2$  showed a notable and broad peak near 22° (Qian et al. 2015; Catauro et al. 2015; Mahesh et al. 2015), resulting in left moving of the main contribution (200) peak at 22.43° in palm fiber compared to the cellulose crystalline peak. The peak, observed as one broad peak around 15°–16°, is actually divided into two peaks corresponding to (1-10) and (110) planes. Higher crystalline cellulose content gives rise to more distinct of the two peaks here. While the large amount of amorphous compounds (such as lignin, hemicellulose and amorphous cellulose) cause the merging of the two distinct peaks into a single peak (Oudiani et al. 2011; Thygesen et al. 2005).

Crystallinity index ( $I_c$ ) measures the orientation of the cellulose crystals in fiber to the fiber axis. The Segal empirical method (Segal et al. 1959) was adopted to evaluate the crystallinity index of palm fiber. The average crystallite size to (200) lattice plane ( $L_{200}$ ) was calculated by the Scherrer equation used in the literature (He et al. 2007; Oudiani et al. 2011). The crystalline parameters of palm are demonstrated in Table 1. It can be found that palm fiber has 30.52 % crystalline cellulose, apparently lower than that of

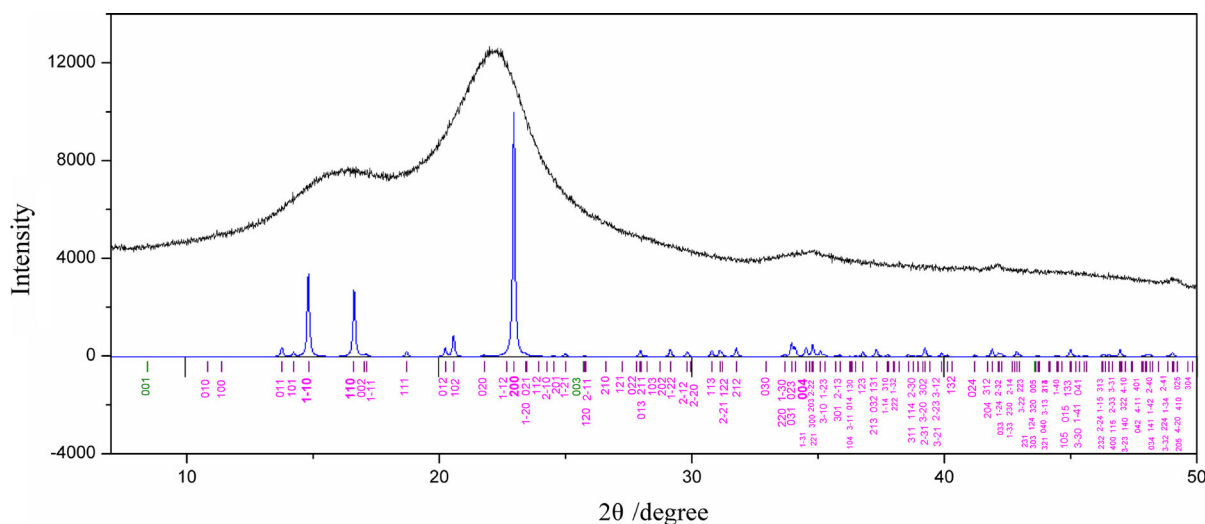


**Fig. 6** X-ray diffractogram of palm fiber

ramie, bamboo and flax fibers (He et al. 2007) and making palm permeable to water and chemicals. Simultaneously, the crystallinity index (36.5 %) and crystalline size (2.5 nm) of palm fiber are both the smallest among the four fibers. The very small crystallites (typically 2–5 nm) will cause considerable peak broadening and serious peak overlap (Thygesen et al. 2005), and the X-ray pattern of palm fiber just present such feature. Furthermore, according to Wang et al. (2010), the relatively poor crystal structure of palm fiber may be due to the large quantity of non-cellulose substances (lignin and hemicellulose) hampering the formation of the cellulose crystalline structure in growing process.

#### Tensile property of palm fiber

The typical stress–strain curves of palm fiber at four different tested lengths are illustrated in Fig. 7a. All the tensile curves present a yielding characteristic, thus indicating excellent elongation property of palm fiber. Tensile strength and strain increase with the decrease in GL from 40 to 10 mm. The curves in Fig. 7a contain three main parts that correspond to three different deformation processes during loading. The first part is the linear region, followed by the nonlinear area in the middle, and then, the final linear region until the fracture. The nonlinear deformation is mainly caused by the fiber’s hierarchical structure and

the orientation change of microfibrils in the cell wall, which leads to amorphous region reconstruction.

Figure 7b–d display the curves, strength, modulus, and strain of palm and other fibers, namely, coir (Tomczak 2007), piassava (d’Almeida et al. 2006), sisal (Munawar et al. 2007), jute (Roy et al. 2012), flax (Charlet et al. 2009), ramie (Cheng et al. 2014), and bamboo (Yu et al. 2014). Considering the similar structural features, palm, coir, and piassava exhibit similar tensile behaviors with a clear nonlinear region following the initial linear portion, whereas the other fibers are prominent in stiffness because their curves are nearly entirely linear. Based on the values in the obtained histograms, despite the changes in indexes along with different GLs, the tensile strength and Young’s modulus of palm family fibers are lower, whereas their strain is significantly higher, than those of other natural cellulosic fibers (sisal, jute, flax, bamboo, and ramie). Palm fiber exhibits low strength but excellent strain property because its low cellulose content and crystallinity, and hierarchical composite structure. According to Greenberg et al. (1989), a significant relationship exists between fiber strength and cellulose content. At room temperature, strength depends on the cellulose content of the fiber because microfibrils are the main support units in fiber cells. Thus, low cellulose content leads to low strength. In addition, the helically oriented cellulose microfibrils of the secondary cell wall determine the axial strength and stiffness of the fiber (Andersons et al. 2011),



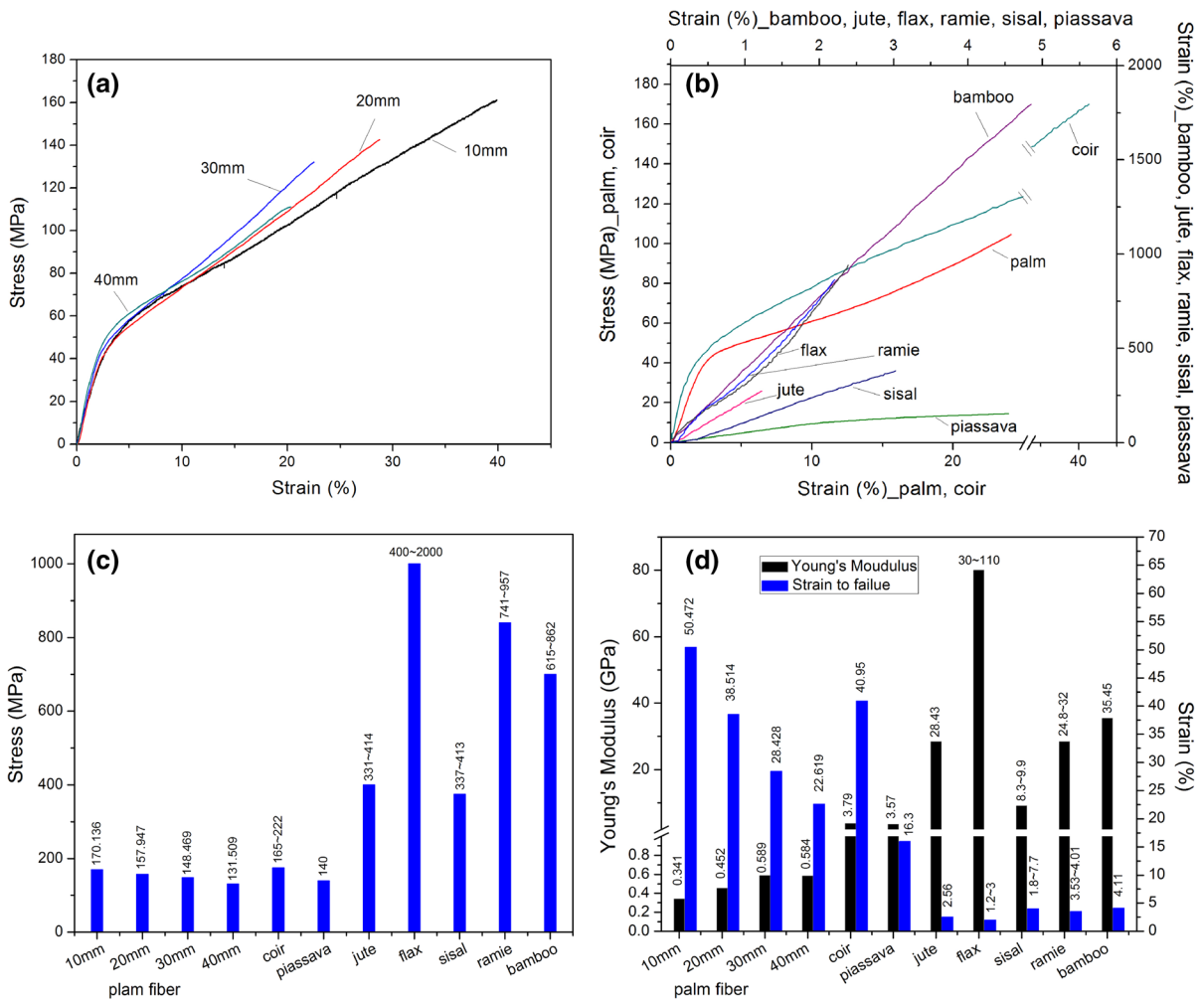


**Fig. 7** Tensile characteristics of palm fiber and other natural fibers

because the microfibril angle of bast fiber is calculated to be approximately 6° smaller than that of palm fiber (>35°; Zhai 2010), and thus, bast fiber exhibits high strength and stiffness (Fig. 7). Given its unique inner structure, palm fiber can exhibit delamination within and between hollow fiber cells during the loading process, thereby decreasing its rupture speed and causing high elongation. Thus, the stress–strain curve of palm fiber varies with yielding area.

According to ASTM D 3379-75, system compliance should be determined experimentally for a given test machine and grip system. Considering that Young’s modulus is independent of GL (d’Almeida et al. 2006), and based on various modulus values with different GLs (Fig. 7), the test results are influenced by test

system compliance. To eliminate the contribution of the test system, Eq. (2) is used to compute test system compliance (*c*) under the relationship of loading force versus displacement behavior at various GLs.

$$\frac{\Delta L}{F} = \left(\frac{1}{ES}\right)l + c \tag{2}$$

where  $\Delta L$  is the displacement of the crosshead during testing, *F* is the loading force, *E* is the Young’s modulus, *S* is the cross-sectional area of the as-tested fiber, and *l* is the GL. Thus, a line of  $\Delta L/F$  versus *l* is established from Eq. (2) with an intercept of *c* and a slope of  $1/ES$ .

Figure 8a demonstrates the linear relationship in Eq. (2). From the plot, *c* = 0.26088 and

$1/ES = 0.01783$  are determined. The corrected Young's modulus values are larger than the uncorrected values (Fig. 8b). Hence, the compliance contribution of the test system results in a lower Young's modulus and a higher strain (large displacement) from the stress–strain behavior.

Palm fiber exhibits variability in tensile strength as it decreases with increasing GL (Fig. 7), which is a common characteristic of natural fibers (Guo et al. 2014; Tomczak 2007). This variability is related with the distribution and size of defects within the fiber or on the fiber surface at various test lengths. The Weibull model is a widely used method to describe such variability by ranking relative fiber strength versus the failure probability (Andersons et al. 2011; Chawla et al. 2005; Silva et al. 2008; Kerr et al. 2005).

Although the two-parameter Weibull distribution is commonly applied to model fiber tensile behavior, it is unsuitable when complying with the experimental data of strength variation with GL (Andersons et al. 2011; Xia et al. 2009). Instead, the modified Weibull model shown in Eq. (3) is precise and suitable for measuring strength variability.

$$P = 1 - \exp\left\{-\left(\frac{L}{L_0}\right)^\gamma \left(\frac{\sigma}{\sigma_0}\right)^m\right\}, \quad 0 < \gamma < 1 \quad (3)$$

where  $\gamma$  denotes fiber diameter variations,  $L$  is the test length,  $L_0$  is the reference length (identified as 1 in this study),  $\sigma_0$  is the characteristic strength or scale parameter, and  $m$  is the Weibull modulus that indicates the scatter degree of fiber strength. In the present

study,  $\gamma$  is calculated by using the method described in literature (Xia et al. 2009). Probability  $P$  is estimated by using Eq. (4):

$$P = \frac{n}{N + 1} \quad (4)$$

which corresponds to the fracture probability of  $n$ th strength value and  $N$  is the total number of fibers tested.

The parameters are estimated by linear regression (Fig. 9). The Weibull modulus  $m$  decreases with increasing GL. Given that the Weibull modulus reflects strength variability, a high Weibull modulus  $m$  indicates low variability in fiber strength. In Fig. 9,

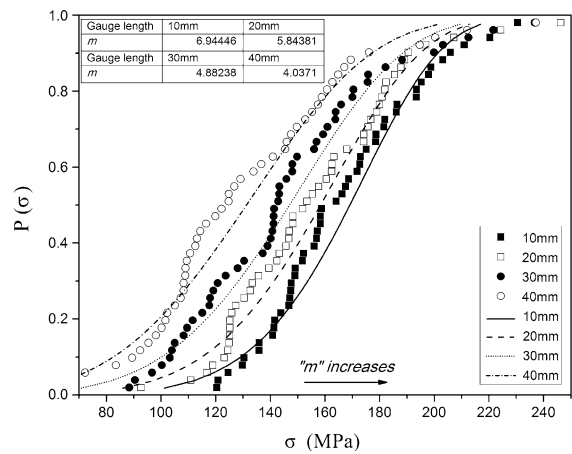


**Fig. 9** The distribution of fiber strength: *dot* corresponds to experimental data, *line* corresponds to Weibull values

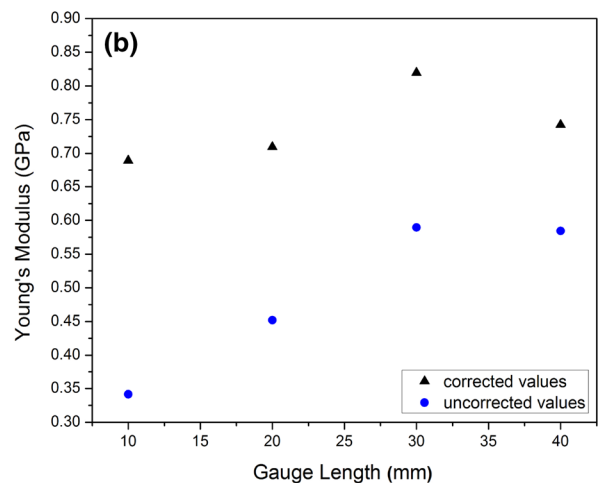
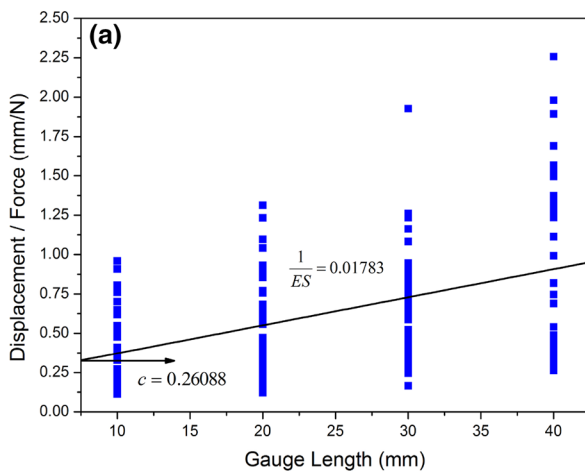


**Fig. 8** **a** The linear plot of normalized displacement versus gauge length; **b** the corrected and uncorrected values of Young's modulus

the strength values of short GL express low variability and high uniformity corresponding to the relative Weibull modulus. This phenomenon is supported by the distribution status of dots. Furthermore, the values obtained from the modified Weibull model [Eq. (3)] are close to the experimental data. Thus, the modified Weibull model can be used to study palm fiber tensile behavior and predict the strength accurately.

Absorption property

Figure 10 presents the moisture absorption and liberation curves. The initial speeds of moisture absorption and liberation are both high, and the

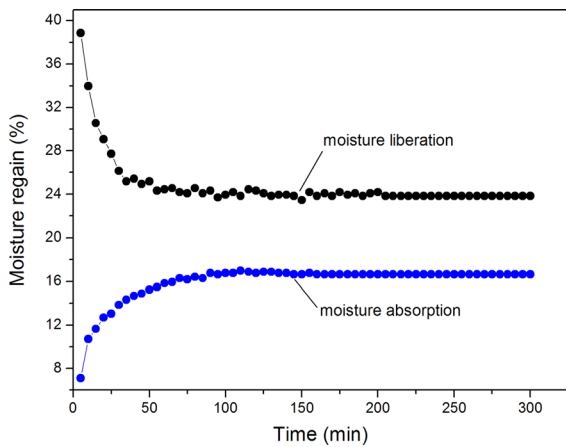


**Fig. 10** The moisture absorption and moisture liberation curve of palm fiber

curves decrease from 35 to 90 min. The fibers reach moisture sorption equilibrium after 4–5 h. The moisture regain of palm fiber that is obtained from moisture absorption/liberation is 16.65/23.83 %, respectively, which is significantly higher than those of cotton (7.48/9.26 %) and flax (8.51/10.34 %). Low crystallinity, rough morphology, and abundant hollow fiber cells contribute to the moisture absorption property of palm fiber. In addition, the relatively high hemicellulose content of palm fiber is responsible for its high-level moisture regain.

Given that palm fiber has abundant hollow cells and exhibits a porous cross section (Figs. 3, 4), the experimental method (GB/T 9995-1977) roughly provides an in-depth discussion of the microscopic morphology of palm fiber. To obtain additional information on the special structure of palm fiber, palm fiber was carbonized at 380 °C for 1 h under isolated oxygen condition. The porous and adsorption characteristics of palm fiber were determined by obtaining the nitrogen adsorption–desorption isotherm

**Table 2** Porosity characteristics of palm, coir and piassava fibers

Sample	BET (m <sup>2</sup> /g)	Pore diameter (nm)	Pore volume (cm <sup>3</sup> /g)
Palm carbon	206.6039	2.02514	0.1046
coir	702	–	0.5317
piassava	1	–	–

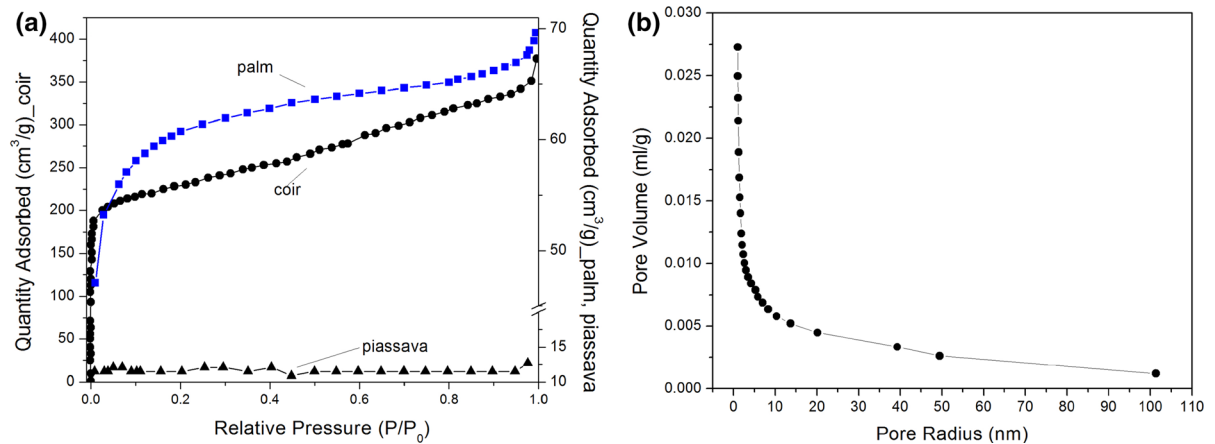


**Fig. 11** **a** The adsorption isotherm linear plot of palm, coir and piassava activated carbon; **b** the adsorption pore distribution of palm activated carbon

at 77.276 K with an ASAP 2020 apparatus (Micromeritics Instrument Corporation, USA).

Figure 11 presents the adsorption isotherm plot and pore distribution of carbonized palm fiber. Total BET surface area, pore diameter, and volume are given in Table 2. The adsorption volume increases from the adsorption isotherm of palm fiber with increasing relative pressure. Such performance indicates good porous character and adsorption property. The N<sub>2</sub> adsorption isotherm (Fig. 11a) of carbonized palm fiber corresponds to an intermediate type between types I and II, which is similar to coir char (Sing et al. 1985; Yang and Peng 2010). The determined BET surface area (206.6 m<sup>2</sup>/g) is lower than that of coir (702 m<sup>2</sup>/g) because the majority of pores in carbonized palm fiber are mesopores (diameter: 2–50 nm), whereas coir chars have a micropore volume of 66 %.

During the preparation of activated carbon, the activation process can further open, widen, and create new pores, as well as merge breakage pores, thus improving the porosity, pore volume, and BET surface of the fiber and optimizing its adsorption property (Avelar and Bianchi 2010). Although piassava fiber presents advantages in structure, untreated piassava exhibits nearly no adsorption volume (Fig. 11a). By contrast, carbonized coir and palm fiber demonstrate excellent adsorption property and unique porous structure. Palm fiber can be an effective adsorbing material after activation.

## Conclusions

Palm fiber is subcylindrical with abundant fiber cells in cross section and Si-dots on surface. It contains only 28.16 % cellulose, lower than bamboo, flax and ramie fibers, but very high lignin. The cellulose in palm fiber is determined as I<sub>β</sub>-dominant type with considerably smaller crystallinity, crystallinity index and crystallite size by FTIR spectra and XRD analysis. Such composition and crystal structure give palm fiber special properties. Palm fiber shows yielding character, varying Young's modulus and the tensile strength decrease with increasing gauge length. To eliminate the influence of test machine compliance, Young's modulus is corrected. Modified Weibull could be used to study strength variability and predict fiber strength accurately. The result of the N<sub>2</sub> adsorption experiment

indicates the mesopore structure and good adsorption property of carbonized palm fiber.

**Acknowledgments** This work was supported by the Science Foundation of Southwest University (SWUB2008049), the Fundamental Research Funds for the Central Universities (XDJK2012D008, XDJK2013A021 and XDJK2015D006) and the Postgraduates Scientific Research Innovation Project in Chongqing (CYB14057).

## References

- Andersons J, Poriķe E, Spārņiņš E (2011) Modeling strength scatter of elementary flax fibers: the effect of mechanical damage and geometrical characteristics. *Compos A* 42:543–549
- Avelar FF, Bianchi ML (2010) The use of piassava fibers (*Attalea funifera*) in the preparation of activated carbon. *Bioresour Technol* 101:4639–4645
- Baley C (2002) Analysis of the flax fibers tensile behaviour and analysis of the tensile stiffness increase. *Compos A* 33: 939–948
- Belaadi A, Bezazi A, Bourchak M (2013) Tensile static and fatigue behaviour of sisal fibres. *Mater Des* 46:76–83
- Cantero G, Arbelaiz A, Mondragon I (2003) Effects of fiber treatment on wettability and mechanical behaviour of flax/polypropylene composites. *Compos Sci Technol* 63: 1247–1254
- Catauro M, Bollino F, Papale F, Gallicchio M, Pacifico S (2015) Influence of the polymer amount on bioactivity and biocompatibility of SiO<sub>2</sub>/PEG hybrid materials synthesized by sol-gel technique. *Mater Sci Eng C* 48:548–555
- Charlet K, Eve S, Jernot JP (2009) Tensile deformation of a flax fiber. *Proced Eng* 1:233–236
- Chawla N, Kerr M, Chawla KK (2005) Monotonic and cyclic fatigue behavior of high performance ceramic fibers. *J Am Ceram Soc* 88:101–108
- Cheng L, Zhang TH, Guo M (2014) Structural characteristics and properties of windmill palm leaf sheath fiber. *Wood Fiber Sci* 46:270–279
- Christina PJ, Rudall PJ, Gregory M (2004) Systematics and biology of silica bodies in monocotyledons. *Bot Rev* 69:377–440
- Cordeiro N, Gouveia C, Moraes AGO (2011) Natural fibers characterization by inverse gas chromatography. *Carbohydr Polym* 84:110–117
- d'Almeida JRM, Aquino RCMP, Monteiro SN (2006) Tensile mechanical properties morphological aspects and chemical characterization of piassava (*Attalea funifera*) fibers. *Compos A* 37:1473–1479
- Dai Z (2008) The design of a new kind of fiber mattress based on composites and its mechanics analysis. *Sci Technol Innov Her* 12:150–151
- Devshony S, Eteshola E, Shani A (1992) Characteristics and some potential applications of date palm seeds and seed oil. *JAOC* 69:595–597
- Focher B, Palma MT, Canetti M, Torri G, Cosentino C (2001) Structural differences between non-wood plant celluloses:

- evidence from solid state NMR, vibrational spectroscopy and X-ray diffractometry. *Ind Crops Prod* 13:193–208
- French AD (2014) Idealized powder diffraction patterns for cellulose polymorphs. *Cellulose* 21:885–896
- Ganner T, Aschl T, Eibinger M (2014) Tunable mixed amorphous-crystalline cellulose substrates (MACS) for dynamic degradation studies by atomic force microscopy in liquid environments. *Cellulose* 21:3927–3939
- Greenberg AR, Mehlig A, Lee M (1989) Tensile behaviour of grass. *J Mater Sci* 24:2549–2554
- Guo M, Zhang TH, Chen BW (2014) Tensile strength analysis of palm fiber leaf sheath fiber with Weibull distribution. *Compos A* 62:45–51
- He JX, Tang YY, Wang SY (2007) Differences in morphological characteristics of bamboo fibers and other natural cellulose fibers: studies on X-ray diffraction, solid state  $^{13}\text{C}$ -CP/MAS NMR, and second derivative FTIR spectroscopy data. *Iran Polym J* 16:807–818
- Jiang XM, He WP (1992) Concise identification of infrared spectroscopy. Guangxi Normal University Press, Guilin
- Kerr M, Chawla N, Chawla KK (2005) Cyclic fatigue of high performance fibers. *JOM* 2:67–70
- Li RQ, Song JC (2005) Measuring techniques for textile materials. Donghua University Press, Shanghai
- Mahesh KPO, Kuo DH, Huang BR (2015) Facile synthesis of heterostructured Ag-deposited  $\text{SiO}_2/\text{TiO}_2$  composite spheres with enhanced catalytic activity towards the photodegradation of AB 1 dye. *J Mol Catal A Chem* 396:290–296
- Maunder M, Lyte B, Dransfield J (2001) The conservation value of botanic garden palm collections. *Biol Conserv* 98:259–271
- Methacanon P, Sumransin N (2010) Properties and potential application of the selected natural fibers as limited life geotextiles. *Carbohydr Polym* 82:1090–1096
- Mortazavi SM, Moghadda MK (2010) An analysis of structure and properties of a natural cellulosic fiber (Leafiran). *Fibers Polym* 11:877–882
- Munawar SS, Umemura K, Kawai S (2007) Characterization of the morphological, physical, and mechanical properties of seven nonwood plant fiber bundles. *J Wood Sci* 53:108–113
- O'Sullivan AC (1997) Cellulose: the structure slowly unravels. *Cellulose* 4:173–207
- Oudiani AE, Chaabouni Y, Msahli S, Sakli F (2011) Crystal transition from cellulose I to cellulose II in NaOH treated *Agave americana* L. fibre. *Carbohydr Polym* 86:1221–1229
- Qian TT, Li JH, Ma HG, Yang J (2015) The preparation of a green shape-stabilized composite phase change material of polyethylene glycol/ $\text{SiO}_2$  with enhanced thermal performance based on oil shale ash via temperature-assisted sol-gel method. *Sol Energy Mater Sol Cells* 132:29–39
- Roy A, Chakraborty S, Kundu SP (2012) Improvement in mechanical properties of jute fibres through mild alkali treatment as demonstrated by utilisation of the Weibull distribution model. *Bioresour Technol* 107:222–228
- Segal L, Creely L, Martin AE, Conrad CM (1959) An empirical method for estimating the degree of crystallinity of native cellulose using X-ray diffractometer. *Text Res J* 29:786–794
- Silva FA, Chawla N, Toledo Filho RD (2008) Tensile behavior of high performance natural (Sisal) fibers. *Compos Sci Technol* 68:3438–3443
- Silva FA, Chawla N, Filho RDT (2009) An experimental investigation of the fatigue behavior of sisal fibers. *Mater Sci Eng A* 516:90–95
- Silva FA, Chawla N, Toledo Filho RD (2010) Mechanical behavior of natural sisal fibers. *J Biobased Mater Bioenergy* 4:106–113
- Sing KSW, Everett DH, Haul RAW (1985) Reporting physisorption data for gas/solid systems with special reference to the determination of surface area and porosity. *Pure Appl Chem* 57:603–619
- Sugiyama J, Persson J, Chanzy H (1991) Combined infrared and electron diffraction study of the polymorphism of native cellulose. *Macromolecules* 24:2461–2466
- Summerscales J, Dissanayake PJ, Virk S (2010) A review of bast fibers and their composites. Part 1: fibers as reinforcements. *Compos A* 41:1329–1335
- Thygesen A, Oddershede J, Lilholt H, Thomsen AB, Ståhl K (2005) On the determination of crystallinity and cellulose content in plant fibers. *Cellulose* 12:563–576
- Tomczak F (2007) Studies on lignocellulosic fibers of Brazil. Part II: morphology and properties of Brazilian coconut fibers. *Compos A* 38:1710–1721
- Wang YP, Wang G, Cheng HT, Tian GL, Liu Z, Xiao QF, Zhou XQ, Han XJ, Gao XS (2010) Structures of bamboo fiber for textiles. *Text Res J* 80:334–343
- Xia ZP, Yu JY, Cheng LD (2009) Study on the breaking strength of jute fibers using modified Weibull distribution. *Compos A* 40:54–59
- Yang KB, Peng JH (2010) Preparation of high surface area activated carbon from coconut shells using microwave heating. *Bioresour Technol* 101:6163–6169
- Yu Y, Wang HK, Lu F (2014) Bamboo fibers for composite applications: a mechanical and morphological investigation. *J Mater Sci* 49:2559–2566
- Zhai S (2010) Structural, chemical and physical properties of palms fiber. Dissertation, Nanjing Forestry University
- Zhang TH, Li XL, Cheng L (2010) Properties and application status of palm fiber. *Tech Text* 6:35–38